

Observation of high-order quantum resonances in the kicked rotor

J.F. Kanem^{1,2}, S. Maneshi^{1,2}, M. Partlow^{1,2}, M. Spanner^{1,3} and A.M. Steinberg^{1,2}

¹*Centre for Quantum Information & Quantum Control*

²*Institute for Optical Sciences & Department of Physics, University of Toronto,
60 St. George Street, Toronto, Ontario, Canada M5S 1A7 and*

³*Chemical Physics Theory Group, Department of Chemistry,
University of Toronto, 80 St. George Street, Toronto, Ontario, Canada M5S 3H6*

(Dated: April 7, 2006)

Quantum resonances in the kicked rotor are characterized by a dramatically increased energy absorption rate, in stark contrast to the momentum localization generally observed. These resonances occur when the scaled Planck's constant $\tilde{h} = \frac{r}{s} \cdot 4\pi$, for any integers r and s . However only the $\tilde{h} = r \cdot 2\pi$ resonances are easily observable. We have observed high-order quantum resonances ($s > 2$) utilizing a sample of low temperature, non-condensed atoms and a pulsed optical standing wave. Resonances are observed for $\tilde{h} = \frac{r}{16} \cdot 4\pi$ for integers $r = 2 - 6$. Quantum numerical simulations suggest that our observation of high-order resonances indicates a larger coherence length than expected from an initially thermal atomic sample.

PACS numbers: 05.45.Mt, 32.80.Pj, 32.80.Lg

A rotor subjected to a periodically pulsed sinusoidal potential ("kicked rotor") is one of the most widely studied paradigms of chaotic dynamics. Ever since the qualitative differences between the classical kicked rotor and the quantum kicked rotor (QKR) became evident [1], the QKR has proven to be a rich system for studying quantum-classical correspondence, decoherence, and quantum dynamics in general. To this day the study of the standard QKR as well as alternative kicked rotor Hamiltonians[2, 3] is an actively pursued field. Much of the early work was done through theoretical and numerical analysis, with one of the more important discoveries being the realization that momentum localization in the QKR can be thought of as a form of Anderson localization[4]. An experimental breakthrough in the field came when laser cooling and optical trapping of atoms allowed the use of optical lattices as a linear momentum analogue of the QKR. This led to the observation of some of the theoretical predictions such as momentum localization[5] as well as studies of decoherence[6] and interesting results arising from modifications to the Hamiltonian of the QKR[7, 8].

Quantum resonances[5, 9] are another aspect of the QKR which have been of experimental interest recently: for certain parameters, heating is greatly enhanced in contrast to the momentum localization usually present in the quantum kicked rotor. In the presence of gravity or other linear potentials one sees accelerator modes[10], similar to quantum resonances except that there is an increase in average momentum as well as momentum spread. Like other aspects of the quantum kicked rotor, quantum resonances are useful for studying quantum-classical correspondence. Work has gone into studying the effect in the presence of noise and the competition with momentum localization and the resonances[11].

Here we present experimental observation of quantum resonances utilizing a sample of cold thermal rubidium atoms in an optical lattice. Specifically, we re-

port our observation of high-order quantum resonances. There have been studies of high-order accelerator modes previously[12] as well as a concurrent observation of high-order resonances in a Bose-Einstein condensate[13]. In all previous experiments with nondegenerate atoms, the higher-order resonances were absent.

The Hamiltonian for the atom optics realization of the delta kicked rotor is

$$H = \frac{p^2}{2m} + \frac{U_0}{2} (1 + \cos(2k_L x)) \sum_n \delta\left(\frac{t}{T} - n\right) \quad (1)$$

where U_0 is the strength of the sinusoidal kick, $2k_L$ is the reciprocal lattice vector of the potential and T is the period of the train of delta kicks. It is convenient to express this as a scaled dimensionless Hamiltonian:

$$\tilde{H} = \frac{\tilde{p}^2}{2} + \chi (1 + \cos(\theta)) \sum_n \delta(\tilde{t} - n) \quad (2)$$

where $\tilde{p} = 2Tk_L p/m$, $\theta = 2k_L x$, $\tilde{t} = t/T$, $\chi = 2U_0 k_L^2 T^2/m$, and $\tilde{H} = H 4T^2 k_L^2/m$.

The scaled quantum Schrödinger's equation is

$$i\tilde{h} \frac{\partial}{\partial \tilde{t}} \psi = -\frac{\tilde{h}^2}{2} \frac{\partial}{\partial \tilde{\theta}} \psi + \chi (1 + \cos \theta) \sum_n \delta(\tilde{t} - n) \psi \quad (3)$$

where $\tilde{h} = 4T k_L^2 \hbar/m$ is the scaled Planck's constant. This effective Planck's constant is a measure of the magnitude of the quantized momentum transfer due to the lattice ($2\hbar k_L$), relative to the momentum required to move one lattice spacing in one kick period, T . Its value determines how quantum-mechanically the system behaves and whether or not quantum resonances are observed.

Quantum resonances occur when $\tilde{h} = \frac{r}{s} \cdot 4\pi$, where r and s are integers. Note that for a given experimental setup \tilde{h} is only sensitive to the kick period, T ,

which can be controlled with great precision. These resonances can be thought of as a rephasing of the momentum states coupled by the lattice potential, whose momenta differ by a multiple of $2\hbar k_L$. Indeed, in the delta kick limit, the condition above can be found by setting the phase between two states accumulated between successive delta kicks to some integer multiple of 2π : $\Delta\phi_a - \Delta\phi_b = (a^2 - b^2) 2\hbar k_L^2 T/m = (a^2 - b^2) \frac{\hbar}{2} = q \cdot 2\pi$, or $\tilde{h} = \frac{q}{(a^2 - b^2)} 4 \cdot \pi = \frac{q}{s} \cdot 4\pi$, recognizing that for any integers a and b , $(a^2 - b^2)$ is also an integer. When this is satisfied for $s = 1$, all coupled momentum states rephase. These first order quantum resonances are related to the revivals of the wavepackets; if the time between kicks is a multiple of the revival time, all the kicks add coherently. This leads to a linear growth in the width of the momentum distribution and quadratic energy growth with kick number, n [14]. This is in contrast to the chaotic situation which arises when the position of the particle for successive kicks is essentially uncorrelated and the energy growth is linear. For the case of $s > 1$, the resulting high-order resonances are a manifestation of the fractional revivals, in which some but not all of the eigenstates rephase, and the wavepacket recoalesces, split into s identical copies.

In the experimental realization the delta kick train is replaced with a train of square pulses of finite width t_p : $\Delta_n(\tilde{t}) = \Theta(\tilde{t} - n) - \Theta(\tilde{t} - \frac{t_p}{T} - n)$, where $\Theta(\tilde{t})$ is the Heaviside step function. Equation (3) then becomes

$$\tilde{h} \frac{\partial}{\partial \tilde{t}} \psi = -\frac{\tilde{h}^2}{2} \frac{\partial^2}{\partial \tilde{\theta}^2} \psi + \kappa \frac{T}{t_p} (1 + \cos \theta) \sum_n \Delta_n(\tilde{t}) \psi \quad (4)$$

where $\kappa = 2Tk_L^2 V_0 t_p/m$ is the stochasticity parameter and V_0 is the energy depth of the lattice potential. In the classical kicked rotor this stochasticity parameter completely defines how chaotic the behavior of the system is.

There are also classical resonances which result in increased energy absorption of the system. A key difference is the condition required; $\kappa = \sqrt{(n \cdot 2\pi)^2 + 16}$ for integer $n > 0$ [15, 16], showing a dependence not solely on the kick period, but also on the strength of the kicks, indicating a Newtonian effect completely independent of \tilde{h} .

Our optical lattice is formed in the vertical direction by two laser beams of wavelength $\lambda = 780$ nm intersecting at an angle of $\gamma = 49.0^\circ \pm 0.2^\circ$ resulting in a laser intensity interference pattern of the form $I(x) = I_0 \cos^2(\frac{2\pi}{\lambda} x \sin(\gamma/2))$. The lattice is detuned by $\Delta \simeq 2\pi \cdot 20$ GHz from the $F = 3 \Rightarrow F' = 4$ D2 trapping line of ^{85}Rb , far enough to be treated as a conservative potential. The spatial lattice period is $l = \frac{\lambda}{2 \sin(\gamma/2)} = 0.940 \mu\text{m} \pm 0.004 \mu\text{m}$. The resulting light shift on the atoms produces a potential $V(x) = I(x) \frac{\hbar \Gamma^2}{4\Delta I_s}$ where Δ is the detuning of the laser from the atomic resonance and Γ and I_s are the natural linewidth and saturation

intensity, respectively, of the atom. In accordance with the kicked rotor model this potential can be expressed as $V(\theta) = V_0 (1 + \cos \theta)$ where $V_0 = \frac{I_0 \hbar \Gamma^2}{I_s 8\Delta}$, $\theta = 2k_L x$ and $k_L = \frac{2\pi}{\lambda} \sin(\gamma/2)$.

We prepare for our experiment by loading a shallow optical lattice from a magneto-optical trap (MOT) of rubidium. While the MOT is still present the lattice laser beams are turned on so that subsequent molasses cooling is done in the presence of the lattice, leading to a higher loading efficiency[17]. This initial lattice is tailored to have a depth of $\sim 19E_r = k_B \cdot 605$ nK where $E_r = \frac{\hbar^2 k_L^2}{2m} \approx k_B \cdot 32$ nK is the effective recoil energy. For our lattice geometry this depth supports two bound states. Because of the vertical orientation of the lattice any unbound atoms will fall out of the interaction region due to gravity. After $\gtrsim 10$ ms only atoms in the two bound states remain, at kinetic temperatures of $(\Delta p)^2/k_B \sim 120$ nK and ~ 360 nK for the ground and first excited states respectively, making for a very cold sample of atoms (~ 240 nK). Time-of-flight measurements are limited by the time it takes for the atomic sample to fall out of the observation region. As a result, this ~ 240 nK is the upper bound which we can place experimentally on the initial atom cloud temperature. This low temperature is to be contrasted with the experiments of most previous work on the subject of quantum resonances which have a molasses-cooled atomic cloud of temperature on the order of several microKelvins. Since the coherence length in a molasses, from which our lattice is loaded, is smaller than an optical wavelength, we do not expect any coherence between lattice wells despite this low temperature. Within each well there is an incoherent mixture of the two bound states. In other words the bands of the lattice are expected to be completely and incoherently filled.

The presence of gravity also adds a tilt to the potential of $3.0E_r$ per spatial lattice period. This tilt would completely alter the dynamics of the kicked rotor in a manner which is interesting[10] but quite different from the theory outlined above. To overcome this we accelerate the lattice downward at g , putting the whole experiment in free fall, thus getting rid of the potential tilt. This is done by frequency-shifting each of the lattice beams by acousto-optic modulators (AOMs). The frequency of the radiofrequency (RF) power driving each AOM is independently controlled by a programmable function generator. By linearly ramping the relative frequency difference between each RF signal, we can accelerate the lattice. The relative frequency difference actually undergoes discrete frequency jumps of 105 Hz every 10 μs . Trial reductions of the granularity by reducing the time between frequency jumps to 5 μs and then 1 μs had no effect on the results. The uncertainty in the lattice angle between lattice beams translates to an uncertainty in the acceleration being applied to the lattice of 0.07 m/s^2 .

The temporal modulation of the lattice potential for the pulse train is done by modulating the laser intensity,

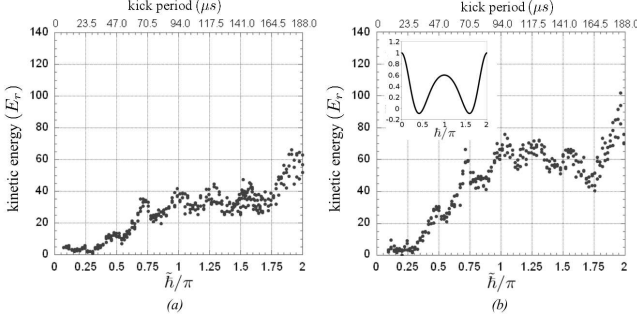


FIG. 1: Experimental graphs showing energy in recoil energies, E_r , versus \hbar/π , and period, T , both with a kick number of 16 (a) Kick strength of $k = 1.23$. High order resonances are seen for $\tilde{h} = \frac{r}{16} \cdot 4\pi$ for $r = 2 - 6$. (b) Same as (a) but with a kick strength of $k = 1.64$. Background trend is from a general kick strength dependent quantum diffusion rate and is modeled by equation 5 which is shown in figure in the inset for $k = 1.6$.

also controlled with the AOMs. The RF signals to the AOMs are sent through RF switches, which are also controlled with a programmable function generator, allowing for a rise/fall time of the lattice intensity of ~ 200 ns. The width of the kicks, t_p , ranges from 5 to 10 μ s and is used as a control for the kick strength, $k \equiv \kappa/\tilde{h} = \frac{V_0 t_p}{2\hbar}$. Simulations show a very small difference between using true delta pulses and the relatively wide pulses we use for the actual experiment, while the experiment itself has confirmed that there is little effect of varying the pulse width but keeping k constant.

After a train of kicks is applied to the atomic ensemble we perform a time-of-flight measurement. First the ensemble undergoes 32 ms of free expansion, and then an image is recorded by flashing resonant light onto the sample and collecting the scattered light on a CCD camera. From this image the thermal energy of the sample is extracted.

Figure 1a shows a typical graph of the average energy of the atoms after 16 kicks versus kick period and effective Planck's constant. The depth of the kicking potential in this case was $V_0 = 98E_r$ with a pulse width of $t_p = 6$ μ s resulting in a kick strength of $k = \frac{V_0 t_p}{2\hbar} = 1.23$. Figure 1b is a similar graph but with $t_p = 8$ μ s resulting in a kick strength of $k = 1.64$.

The general background trend is a kick strength effect independent of the high-order resonances and can be modeled by the quantum diffusion parameter

$$D(k, \tilde{h}) = \frac{k^2 \tilde{h}^2}{2} \left[\frac{1}{2} - J_2(d) - J_1^2(d) + J_2^2(d) + J_3^2(d) \right] \quad (5)$$

where J_n are n th order Bessel functions and $d \equiv 2k \sin(\tilde{h}/2)$ [15, 18]. The energy increase due to this diffusion is given by $\frac{m}{4k_L^2 T^2} D(k, \tilde{h})$. The result is shown in the inset of figure 2b. This equation does not model the

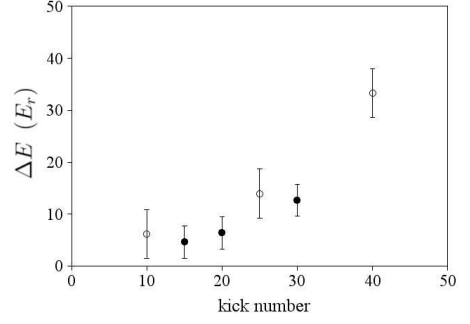


FIG. 2: Magnitude of the $\tilde{h} = \frac{3}{4}\pi$ resonance as a function of kick number. Solid and open circles indicate different sets of experimental data.

decreasing stochasticity ($\kappa = k\tilde{h}$) as $\tilde{h} \rightarrow 0$, explaining its failure to reproduce the vanishing heating rate seen in the experiment.

The experiment was performed for several different parameters in order to verify that the position of the resonances is solely a function of the effective Planck's constant. The kick strength was varied by adjusting the temporal width of the pulses from 6 to 14 μ s, leading to kick strengths from $k = 1.23$ to $k = 2.86$. We see that an increase by more than a factor of two, which would displace classical resonances by the same factor, leaves the high order resonance structure in place to within our experimental error of about ± 2 μ s. These resonances lie at an average period of $T = 45.2 \pm 0.9, 69.0 \pm 1.0, 96.0 \pm 1.4, 120.0 \pm 1.4$, and 147.5 ± 1.0 μ s. These correspond to values of $\tilde{h}/\pi = 0.47 \pm 0.01, 0.72 \pm 0.01, 1, 1.25 \pm 0.02, 1.54 \pm 0.02$. (The position of the central resonance is defined to be precisely 1 because it itself is our most accurate calibration of \tilde{h} .) We identify these as the high order resonances occurring for $\tilde{h} = \frac{r}{16} \cdot 4\pi$, for $r = 2 - 6$.

We also examined the characteristics of the resonances as a function of kick number. The primary trend noted is the clarity of the resonances. Figure 2 shows peak height in energy (over the baseline) of the $\tilde{h} = \frac{3}{4}\pi$ resonance for different kick numbers. In other words, this is the kinetic energy at the resonance minus the energy minimum between resonances. We believe this reflects the narrowing of the resonances with increased kick number.

We have studied these quantum resonances numerically while modeling the experiment with realistic parameters. Figure 3 shows the results of quantum simulations graphing energy absorption in recoil energies after 16 kicks versus kick period (and \tilde{h}/π) for $k = 1.6$. There is a strong sharp resonance at $\tilde{h} = 2\pi$ as well as a higher order one at $\tilde{h} = \pi$, and less well resolved high-order resonances at $\tilde{h} \sim \frac{3}{4}\pi$, among others at $\tilde{h} \sim \frac{r}{s} \cdot 4\pi$ of order $s > 16$. The initial state of 3a is an uncertainty-limited Gaussian momentum distribution, $\psi(x) = \left(\frac{1}{2\pi x_0^2}\right)^{1/4} \exp\left[-\frac{x^2}{4x_0^2}\right]$ with velocity width of $v_0 = \frac{\hbar}{2mx_0} = 3.43$ mm/s. This is the velocity distribution of the ground band of a $19E_r$

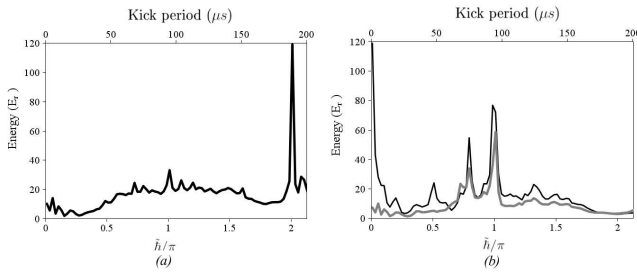


FIG. 3: Numerical simulations showing energy in recoil energies, E_r , versus \hbar/π , and period, T , both with a kick number of 16 and $k = 1.6$. (a): The *rms* spatial distribution of the initial wavefunction is $x_0 = 0.109 \mu\text{m}$ ($v_0 = 3.43 \text{ mm/s}$). (b): Initial distributions with coherence throughout the sample. The grey line has an initial distribution of a sum of in-phase Gaussians, each separated by the lattice spatial period, $l = 0.94 \mu\text{m}$, while that of the black line has a wide initial *rms* spatial width of $x_0 = 1.09 \mu\text{m}$.

deep lattice, a state we can readily prepare[19]. This gives a spatial width of $x_0 = 0.109 \mu\text{m}$ which localizes each wavepacket entirely within one well. There is no defined phase between wavefunctions in adjacent wells.

We find that the initial conditions of the atomic cloud, namely its momentum distribution and coherence properties, have a large effect on the relative strengths of the various high-order resonances. Figure 3b shows the results of two numerical simulations, each having an initial distribution with a coherence length spanning several lattice spatial periods. The initial distribution of the grey line is a sum of Gaussians, weighted by an overall Gaussian envelope. Each individual Gaussian has a spatial distribution width of $x_0 = 0.109 \mu\text{m}$ as in 3a. This makes for a constant phase from well to well throughout the atomic sample; $\psi_0(x) = N \exp\left[-\frac{x^2}{4x_r^2}\right] \sum_n \exp\left[-\frac{(x-n\cdot l)^2}{4x_0^2}\right]$, where N is a normalization constant and $x_r = 1.09 \mu\text{m}$ is the *rms* radius of the overall Gaussian that each individual “cloud” is weighted by. The black line is a single Gaussian with an initial spatial *rms* width of $x_0 = 1.09 \mu\text{m}$ making for a velocity distribution of *rms* width $v_0 = 0.343 \text{ mm/s}$. The result of these distributions show clearly observable resonances. They are visible at $\tilde{h} = \frac{r}{16} \cdot 4\pi$ for $r = 2, 3, 4$

with another one at $\tilde{h} = \frac{1}{5} \cdot 4\pi$. The other obvious difference between figures 3b and 3a is the absence of the resonance at $\tilde{h} = 2\pi$. It is worth noting that in an angular momentum kicked rotor system, as opposed to the optical lattice implementation used here, this resonance at $\tilde{h} = 2\pi$ is never present. This is one of several subtle differences owing to the fact that in the kicked rotor the wavefunction must be cyclic; $\psi(\theta) = \psi(\theta + 2\pi)$. This is only true in the linear momentum analogue of the optical lattice if there is coherence throughout the atomic sample. The initial distribution of figure 3b has this long range coherence put in by hand for the simulation shown in grey, while the extremely low initial momentum spread of the simulation shown in black makes for a long spatial coherence.

It is also worth noting that many small higher-order resonances exist and appear in figure 3a none of them dominating the others. But when the initial distribution has coherence throughout several wells the $\tilde{h} = \frac{r}{16} \cdot 4\pi$ resonances seen in figures 3b grow several times stronger than the others, in qualitative agreement with the experimental observations shown in figures 1a,b. The fact that the numerical simulations do not show clear high-order resonances unless there is long-range coherence suggests that our initial atomic state actually has some phase-coherence between adjacent wells; we are currently investigating this possibility experimentally and theoretically.

In summary we have observed clear high-order resonances in an optical-lattice implementation of the kicked rotor using thermal atoms. Our technique of selecting an extremely cold sample of atoms may explain the fact that we observe these resonances, not previously seen in thermal clouds. We have verified, in accordance with theory, that only the value of the effective Planck’s constant determines the positions of the resonances. In addition our results suggest that there may be long range coherence across the optical lattice, which was loaded from an ensemble of thermal atoms. Future studies will examine the role of inter- and intra-well coherence in the kicked rotor as well as the various mechanisms for such coherence to be developed. Our findings also suggest that the QKR may be of interest as a probe of such coherence.

We would like to thank Paul Brumer and Jiangbin Gong for inspiration and useful discussions. This work was funded by NSERC and PRO.

-
- [1] G. Casati, B.V. Chirikov, F.M. Izraelev, J. Ford, ‘Stochastic Behavior of a Quantum Pendulum Under Periodic Perturbation’, in *Stochastic Behavior in Classical and Quantum Hamiltonian Systems*, (Lecture Notes in Physics **93** Springer (1977).
 - [2] J. Gong, H.J. Wörner, P. Brumer, Phys. Rev. E **68**, 056202 (2003).
 - [3] J. Gong, P. Brumer, Phys. Rev. E **70**, 016202 (2004).
 - [4] S. Fishman, D.R. Grempel, R.E. Prange, Phys. Rev. Lett. **49**, 509 (1982).
 - [5] F.L. Moore, J.C. Robinson, C.F. Bharucha, B. Sundaram, M.G. Raizen, Phys. Rev. Lett. **75**, 4598 (1995).
 - [6] V. Milner, D. A. Steck, W.H. Oskay, M.G. Raizen, Phys. Rev. E **61**, 7223 (2000).
 - [7] H. Lignier, J.C. Garreau, P. Szriftgiser, D. Delande, Europhys. Lett. **69**, 327 (2005).
 - [8] *Effects of a periodically reversed delta kicked rotor* J.F. Kanem, S. Maneshi, M. Partlow, M. Spanner, A.M. Steinberg. In preparation.
 - [9] F.M. Izraelev, D.L. Shepelyansky, Theor. Math. Phys.

- 43**, 553 (1980).
- [10] R.M. Godun, M.B. d'Arcy, M.K. Oberthaler, G.S. Summy, K. Burnett, Phys. Rev. A **62**, 013411 (2000).
 - [11] M.B. d'Arcy, R.M. Godun, M.K. Oberthaler, D. Cassetari, G.S. Summy, Phys. Rev. Lett **87**, 074102 (2001).
 - [12] S. Schlunk, M.B. d'Arcy, S.A. Gardiner, G.S. Summy, Phys. Rev. Lett. **90**, 124102 (2003).
 - [13] C. Ryu, M.F. Andersen, A. Vaziri, M.B. d'Arcy, J.M. Grossman, K. Helmerson, W.D. Phillips, preprint (submitted to Phys. Rev. Lett.).
 - [14] A quadratic energy growth with kick number is actually only seen in the angular momentum version of the kicked rotor. The linear momentum analogue utilized here shows a linear energy growth until momentum localization sets in.
 - [15] A.J. Lichtenberg, M.A. Lieberman, *Regular and Chaotic Dynamics*, Springer, NY, (1992).
 - [16] R. Ishizaki, T. Horita, T. Kobayashi, H. Mori, Prog. Theor. Phys. **85**, 1013 (1991).
 - [17] M. DePue, C. McCormick, S. Winoto, S. Oliver, D. Weiss, Phys. Rev. Lett. **82**, 2263 (1999).
 - [18] D.L. Shepelyansky, Physica **28D**, 103 (1987).
 - [19] J.F. Kanem, S. Maneshi, S.H. Myrskog, A.M. Steinberg, J. Opt. B **7**, S705 (2005).